First preclinical evaluation of mono-[^{123}I]iodohypericin as a necrosis-avid tracer agent

Yicheng Ni[1], Dieter Huyghe[2], Kristin Verbeke[2], Peter A. de Witte[3], Johan Nuyts[4], Luc Mortelmans[4], Feng Chen[1], Guy Marchal[1], Alfons M. Verbruggen[2], Guy M. Bormans[2]

[1] Department of Radiology, University Hospital Gasthuisberg, Leuven, Belgium
[2] Laboratory of Radiopharmaceutical Chemistry, Faculty of Pharmaceutical Sciences, University of Leuven, Herestraat 49, 3000 Leuven, Belgium
[3] Laboratory of Pharmaceutical Biology and Phytopharmacology, Faculty of Pharmaceutical Sciences, University of Leuven, Leuven, Belgium
[4] Department of Nuclear Medicine, University Hospital Gasthuisberg, Leuven, Belgium

Received: 9 May 2005 / Accepted: 14 September 2005 / Published online: 1 February 2006

Abstract. *Purpose:* We have labelled hypericin, a polyphenolic polycyclic quinone found in St. John's wort (*Hypericum perforatum*), with ^{123}I and evaluated mono-[^{123}I]iodohypericin (MIH) as a potential necrosis-avid diagnostic tracer agent.
Methods: MIH was prepared by an electrophilic radioiodination method. The new tracer agent was evaluated in animal models of liver infarction in the rat and heart infarction in the rabbit using single-photon emission computed tomography (SPECT), triphenyltetrazolium chloride (TTC) histochemical staining, serial sectional autoradiography and microscopy, and radioactivity counting techniques.
Results: Using in vivo SPECT imaging, hepatic and cardiac infarctions were persistently visualised as well-defined hot spots over 48 h. Preferential uptake of the tracer agent in necrotic tissue was confirmed by perfect match of images from post-mortem TTC staining, autoradiography (ARX) and histology. Radioactivity concentration in infarcted tissues was over 10 times (liver; 3.51% ID/g in necrotic tissue vs 0.38% ID/g in normal tissue at 60 h p.i.) and over 6 times (myocardium; 0.36% ID/g in necrotic tissue vs 0.054% ID/g in normal tissue; ratios up to 18 for selected parts on ARX images) higher than in normal tissues.
Conclusion: The results suggest that hypericin derivatives may serve as powerful necrosis-avid diagnostic agents for assessment of tissue viability.

Keywords: Hypericin – SPECT imaging – Autoradiography – Radioiodine – Necrosis

Alfons M. Verbruggen (✉)
Laboratory of Radiopharmaceutical Chemistry,
Faculty of Pharmaceutical Sciences,
University of Leuven,
Herestraat 49,
3000 Leuven, Belgium
e-mail: alfons.verbruggen@uz.kuleuven.ac.be
Tel.: +32-16-343732, Fax: +32-16-343891

Eur J Nucl Med Mol (2006) 33:595–601
DOI 10.1007/s00259-005-0013-2

Introduction

Non-invasive "hot spot imaging" and localisation of necrotic tissue may be helpful for the diagnosis of different disorders. This is especially true in the case of ischaemic myocardial injury, where imaging using necrosis-avid agents could help in measuring infarct size. This could allow the rapid use of interventions for myocardial salvage through early identification of the acute event, thereby improving the clinical outcome. Also, other cardiovascular disorders associated with cardiac cell death could be visualised and diagnosed, such as cardiomyopathies, myocarditis and heart transplant rejection [1].

In nuclear medicine, only a limited number of hot spot imaging agents have been used or proposed for diagnosis of necrosis. ^{99m}Tc-pyrophosphate was the first of them and is supposed to bind to necrotic myocardium by targeting calcium phosphate deposited in the mitochondria of infarcted or severely injured myocardial tissue [2]. However, ^{99m}Tc-pyrophosphate scintigraphy has never gained widespread use because of its limited diagnostic accuracy and the relatively poor stability of the tracer agent, which may lead to the in vivo formation of pertechnetate and so result in imaging of the cardiac chambers. More recently, ^{111}In-labelled murine monoclonal antimyosin Fab antibody fragments were introduced for infarct-avid scintigraphy [3, 4]. This so-called ^{111}In-antimyosin has a selective affinity for the intracellular heavy chain of cardiac myosin, which is exposed when the integrity of the sarcolemma is lost as a result of cell damage [5, 6]. It is incorporated in the necrotic myocardium in an inverse relationship to regional flow, with maximum uptake in areas with severe flow impairment, although its uptake is more intense in myocardial

infarcts with reperfusion than in those with persistent coronary occlusion [7]. It was also found useful for detection of acute or chronic diffuse myocardial damage in allograft rejection in cardiac transplantation [8, 9], doxorubicin-induced cardiotoxicity [10], acute myocarditis [11, 12] and various cardiomyopathies [13, 14]. Although ^{111}In-antimyosin has been approved by the FDA for clinical use, the limitation of approved indications to ischaemic heart disease has resulted in cessation of commercial production.

A few years ago, it was observed that the complex of ^{99m}Tc with glucaric acid, a simple dicarboxylic acid sugar, localised in canine reperfused myocardial infarction soon after injection [15]. The tracer agent is supposed to bind to positively charged histones within disintegrated nuclei and reduced subcellular organelle proteins in necrotic myocytes [16]. It has the advantages of a rapid blood pool clearance, a good target to background ratio, and lack of toxicity and antigenicity, and is claimed to have a good sensitivity and specificity for detection of early irreversible myocyte injury. On the other hand, its uptake is limited to the first 9 h after the onset of acute myocardial infarction because of the relatively rapid disintegration of the positively charged histones. Further clinical trials will be required to reveal its real clinical usefulness.

In the field of magnetic resonance imaging (MRI), it has recently been reported that some porphyrin derivatives that were originally developed as tumour-seeking contrast agents [17] have avidity only for non-viable tissues (typically necrosis) instead of viable tumour cells and could therefore be re-categorised as necrosis-avid contrast agents [18–20]. The extraordinary targetability of these agents for necrosis has elicited novel applications for MRI visualisation of acute myocardial infarction [21–32] and therapeutic tissue ablation [33]. Some porphyrin derivatives are also useful as photosensitisers and tumour localisers for photodynamic therapy (PDT) [34]. PDT is a relatively recent modality for the treatment of cancer, which requires combination of a chemical photosensitiser that is preferentially taken up and retained by tumour cells and light of an appropriate wavelength to generate singlet oxygen free radicals out of the photosensitiser [34]. While photofrin-2 represents the commercially available porphyrin derivative that is most frequently used, hypericin (Fig. 1), a polyphenolic polycyclic quinone found in St. John's wort (*Hypericum perforatum*) is regarded as a powerful naturally occurring photosensitiser. It is being applied in PDT under the same principle as that for porphyrin derivatives [35].

Considering the role of hypericin and photofrin-2 in PDT and the recently recognised necrosis avidity of certain porphyrin-derived contrast agents, we hypothesised that hypericin may share the similar properties of preferential uptake and retention in necrotic tissues. For this reason, we have synthesised mono-[^{123}I]iodohypericin (MIH), a ^{123}I-labelled derivative of hypericin (Fig. 1), and evaluated it in an imaging and histomorphological study designed to explore its potential utility as a necrosis-avid tracer agent.

Fig. 1. Chemical structure of hypericin (R=H) and mono-[^{123}I]iodohypericin (MIH) (R=^{123}I)

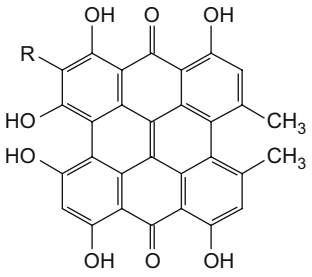

Materials and methods

Synthesis and preparation of mono-[^{123}I]iodohypericin

MIH was synthesised in no-carrier-added form using a standard electrophilic radioiodination method in the presence of peracetic acid and was purified with high-pressure liquid chromatography (HPLC) as described previously [36]. After purification the MIH solution was evaporated to dryness at 60°C under a flow of nitrogen and the tracer agent was redissolved in water/polyethylene glycol (PEG) 400 (8:2, V/V) immediately before injection.

Animal models of necrosis

All animal experiments were conducted with the approval of the institutional ethical committee.

Reperfused hepatic infarction

Three adult Wistar rats weighing 400–450 g were anaesthetised with intraperitoneal injection of pentobarbital (Nembutal; Sanofi Santé Animale, Brussels, Belgium) at a dose of 40 mg/kg. Under laparotomy, reperfused hepatic infarction was induced by temporarily clamping the hilum of the right liver lobes for 3 h. After reperfusion by declamping hepatic inflow, the abdominal cavity was closed with two-layer sutures and the rats were allowed to recover for 8–24 h after the surgery [19, 37]. One rat underwent a sham operation and served as a non-infarcted control.

Occlusive myocardial infarction

A New Zealand adult rabbit weighing about 5 kg was sedated with intramuscular injection of a mixed solution of ketamine hydrochloride (Ketalar; Pfizer, Brussels, Belgium) at 15 mg/kg and xylazine hydrochloride (Rompun; Bayer, Leverkusen, Germany) at 2.5 mg/kg. The animal was then anaesthetised with an intravenous bolus injection of Nembutal at 15 mg/kg followed by i.v. infusion of Nembutal at 0.1 mg/kg per minute through an ear vein. Under a cold-light laryngoscope with no. 1 paediatric blade (Riester; Jungingen, Germany), the animal was intubated with a 3.5-mm endotracheal tube, which was then connected to an artificial ventilator (Mark 7 respirator; Bird Corporation, Palm Springs, CA, USA). Open chest surgery (left posterolateral thoracotomy) was performed. The pericardium was opened to expose the left circumflex coronary artery, which was then permanently ligated with a 3-0 silk suture. The chest was closed after evacuation of the pneumothorax.

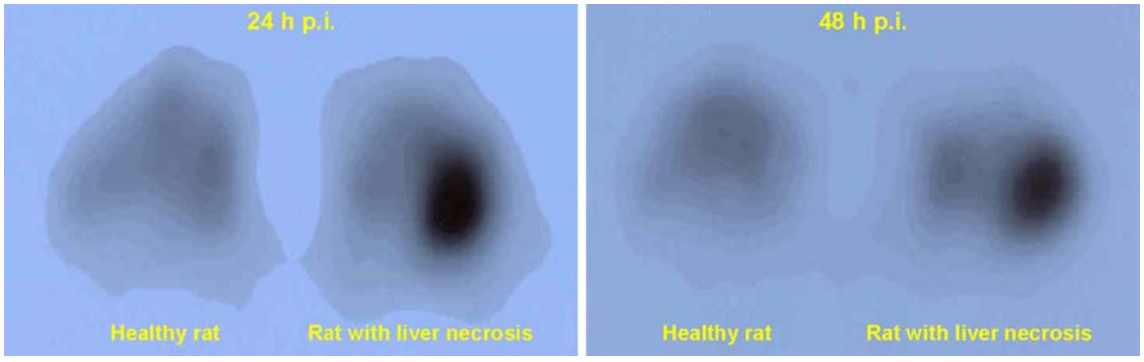

Fig. 2. SPECT transverse section images obtained in normal rats (*left*) and rats with reperfused hepatic infarction (RHI, *right*) at 24 h and 48 h post injection of MIH. The persistent hyperactivity is found only in the infarcted right liver lobe of the rat RHI model, and not in the intact liver lobe of the rat RHI model or in the liver of the sham-operated rat (results not shown)

Tracer administration

Five hours after reperfusion of the hepatic infarction, the rats were intravenously injected with 18.5 MBq of MIH through a tail vein. Five hours after induction of the myocardial infarction, the rabbit was injected with 130 MBq MIH via an ear vein.

SPECT imaging

All imaging measurements were performed using a two-detector gamma camera (E-cam; Siemens Medical Systems, Erlangen, Germany). Each animal was secured to the head-holder of the patient bed with the organ of interest in the centre of the field of view. SPECT projections were collected using the following acquisition parameters: 120 projections over 360° per detector head (step and shoot mode), 25 s per projection, a matrix size of 256×256, a pixel size of 2.4 mm and a non-circular orbit. The images of the rats were reconstructed with filtered back projection, using a ramp filter and cut-off at the Nyquist frequency. The images of the rabbit were reconstructed with maximum-likelihood expectation-maximisation, applying 47 iterations.

In vivo SPECT was conducted under the same anaesthetic regimens as were used for surgery in both the rats and the rabbit. The rats were imaged consecutively during the first 2–3 h, and then 24 and 48 h after injection of MIH. One rat with liver lobe infarction and one sham-operated control rat were placed parallel supine and imaged simultaneously. The rabbit was imaged in a similar fashion but only 24 and 48 h after injection of MIH.

Animal sacrifice and tissue sampling

Forty-eight to 60 h post injection, the animals were sacrificed with an intravenous overdose of Nembutal. The rat liver and rabbit heart were excised. The partially necrotic part of the liver was cut into blocks at a thickness of about 1 cm, which were quickly frozen in isopentane cooled over dry ice to −40°C. The heart was cut perpendicular to the long axis into 5-mm-thick slices starting from the apex.

Histochemical staining

Representative blocks of liver tissue and the slices of heart were immersed in a buffered triphenyltetrazolium chloride (TTC) solution for staining during 10 min at 37°C. After this staining, normal liver and myocardial tissues appeared brick red and the necrotic areas were unstained [22, 24, 27–32]. The TTC-stained specimens were digitally photographed and stored for later imaging–histochemical match.

Ex vivo autoradiography

The frozen liver and heart tissues, adjacent to the tissue sections for TTC staining, were cut at −20°C into 20- to 50-µm serial sections and exposed overnight to a high-performance storage phosphor screen (Super resolution screen; Canberra-Packard, Ontario, Canada). The screen was read using a Phosphor Imager scanner (Cyclone; Canberra-Packard). The images were analysed using Optiquant software (Canberra-Packard). Afterwards, the same sections were stained with haematoxylin-eosin (H&E) using the conventional procedure. These H&E-stained sections were digitally scanned and the obtained images were corrected for brightness and contrast.

Tissue radioactivity counting

Guided by TTC staining, the liver lobes of the rat and heart sections of the rabbit were sampled for normal and necrotic parts, weighed separately and counted for radioactivity using a 3-in. NaI(Tl)

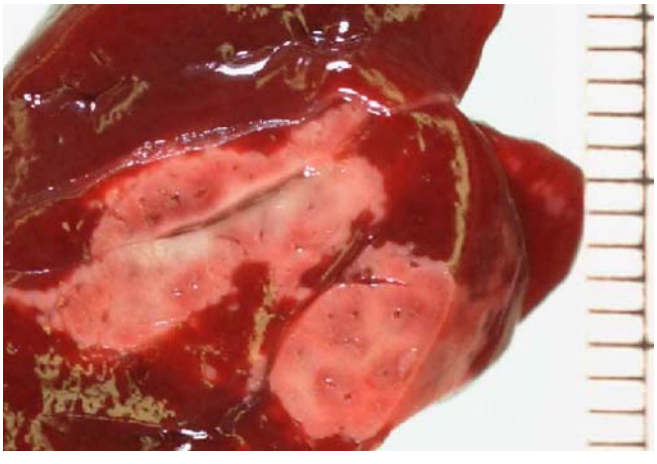

Fig. 3. TTC staining of the liver lobe with focal reperfused infarction. From the 5-mm tissue block adjacent to the slice for autoradiography and histology (Fig. 4), the normal liver tissue (red) and necrotic tissue (pale) were sampled for radioactivity counting

Fig. 4. Comparison of autoradiography (*left*) and H&E staining without (*middle*) and with (*right*) enhanced contrast and brightness of the same 50-µm frozen liver slice containing reperfused infarct from the rat

scintillation detector mounted in a sample changer (Wallac Wizard, Turku, Finland). Corrections were made for background radiation and physical decay during counting. The activity in the normal and infarcted parts of the liver and heart was then expressed as counts per gram tissue.

Results

Liver lobe infarction in rats

SPECT imaging During the first couple of hours after i.v. administration of MIH in both infarcted and normal control rats, a systemic distribution pattern appeared. Higher activity uptake was seen especially in the liver and kidneys as well as in the intestines and urinary bladder, indicating the major elimination pathways of the compound. In comparison with a complete outline of the liver in the normal rat, there was a filling defect at the lower right quadrant of the liver, corresponding to the induced liver infarction. At 24 h and 48 h post injection, on the transverse SPECT image, the uptake of radioactivity in the infarcted liver lobe was apparently much higher than that in the non-infarcted liver lobe and that in the liver of the sham-operated rat (Fig. 2). Residual radioactivity was also shown in the regions of the thyroid and intestines.

Tissue radioactivity counting Sixty hours post injection of the tracer agent, the results of radioactivity quantification of dissected tissues showed high uptake in the necrotic liver lobe of 3.51% ID/g, which was almost 10 times the radioactivity concentration found in normal liver lobes (0.38% ID/g). Furthermore, the amount in the liver lobes of the control rat was comparable to the amount found in the untreated liver lobes of the rat with infarction (0.58% ID/g).

Histochemical staining Figure 3 shows a picture of a 1-cm-thick block of the partially necrotic liver of the rat. After staining with TTC, the reddish normal liver and adjacent pale necrotic tissue could be easily identified, as was confirmed by H&E staining of the 50-µm serial sections taken from the tissue 5 mm next to this slice (Fig. 4).

Ex vivo autoradiography Figure 4 compares the images of autoradiography and H&E staining of the same 50-µm sections. High tracer uptake appears only in the eosino-

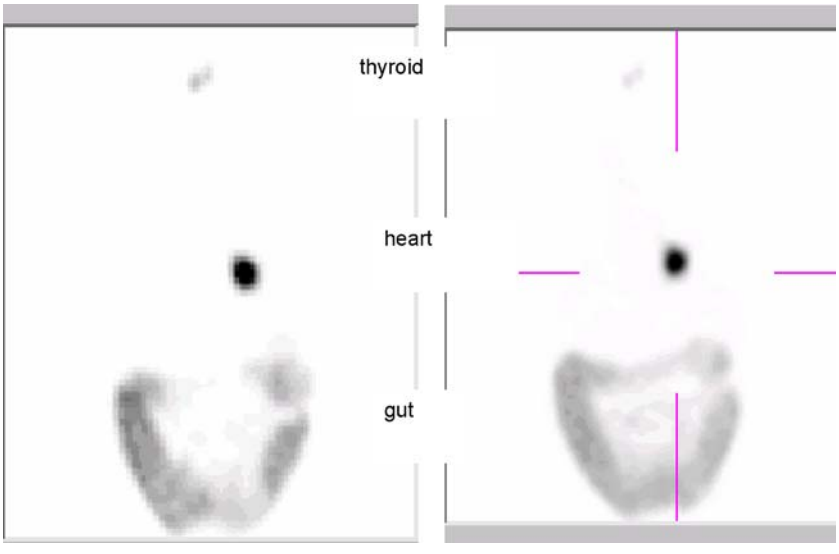

Fig. 5. SPECT images (coronal section) obtained at 24 h (*left*) and 48 h (*right*) post injection of MIH in a rabbit with myocardial infarction. The radioactivity can be persistently found in the heart region and to a lesser extent in the thyroid and gut

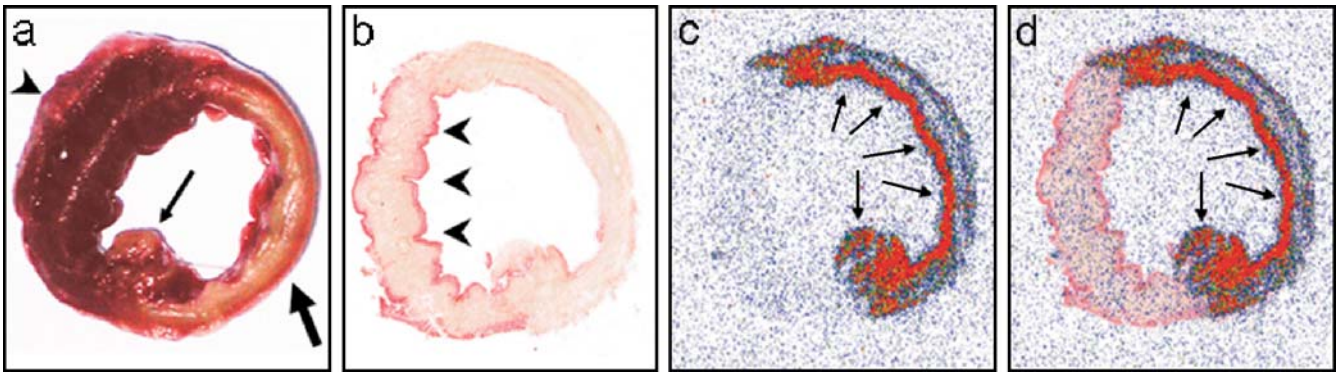

Fig. 6. Ex vivo images of rabbit heart. After TTC staining of a 5-mm-thick slice (**a**), a 50-µm frozen slice (**b**, TTC stained) was obtained. The autoradiographic image (**c**) of this 50-µm slice matched perfectly when overlapped with the image of TTC staining (**d**). **a** On the TTC-stained specimen with right ventricular wall attached (*arrowhead*), the transmural infarction (pale or negatively stained with TTC) involves the entire anterior and lateral wall of the left ventricle (*thick arrow*), including the posterior papillary muscle (*thin arrow*). **b** On the frozen slice with right ventricular wall removed, non-infarcted myocardium (*arrowheads*) at the posterior wall and interventricular septum is stained brick red only superficially with TTC (by the nature of this macroscopic staining technique). **c, d** On autoradiography, a "doughnut" pattern of radioactivity uptake appears only in the infarcted region. However, the highest activity (in red) is found mainly subendocardially and near the lateral border zone, where the tracer is able to diffuse from the blood circulation into this occlusive myocardial infarct (*arrows*)

philic necrotic parts (pink coloured on H&E images), whereas low tracer uptake is found in the (haematoxylinophilic) healthy parts of the liver (purple coloured after H&E staining). The topographic distribution of the radioactivity matches perfectly with that of the necrotic tissue components, suggesting that MIH specifically accumulates in necrotic tissue.

Myocardial infarction in the rabbit

In vivo SPECT imaging Twenty-four and 48 h post injection of MIH in the rabbit with occlusive myocardial infarction, a coronal section view after iterative reconstruction of whole-body SPECT persistently displayed only one hot spot in the anatomical area of the heart. Radioactivity to a much lesser extent could also be seen in the regions of the thyroid and intestines (Fig. 5).

Tissue radioactivity counting TTC staining enabled selective sampling of reddish normal myocardium and whitish infarcted myocardium for radioactivity quantification. At 48 h post injection of the tracer agent, radioactivity concentration in necrotic heart tissue was 0.36% ID/g, which was about 6.6 times the radioactivity concentration found in normal myocardium (0.054% ID/g). The ratio would be even much higher if tissue sampling were to be guided by the outcome of autoradiography in this model of occlusive myocardial infarction (Fig. 6). On the basis of the autoradiographic images, an 18-fold higher radiotracer concentration was found in selected infarcted tissue than in healthy tissue.

Ex vivo histochemical staining and autoradiography Figure 6 compares TTC staining of a 5-mm-thick slice and a 50-µm frozen slice with the corresponding autoradiographic image of this frozen slice and a superposition of the last two images. On the TTC-stained specimen with right ventricular wall attached (Fig. 6a), the transmural infarction involves the entire anterior and lateral wall of the left ventricle, including the posterior papillary muscle (negative staining with TTC). On the frozen slice with right ventricular wall removed (Fig. 6b), the normal myocardium at the posterior wall and interventricular septum are stained only superficially with TTC (by the nature of this macroscopic staining technique). On autoradiography (Fig. 6c,d), a "doughnut" pattern of radioactivity uptake appears only in the infarcted region. However, the highest activity (in red) is found mainly subendocardially and near the lateral border zone, a sign characteristic for occlusive myocardial infarct [38, 39].

Discussion

As hypericin is a polyphenolic polycyclic quinone, it can be labelled efficiently with radioiodine by electrophilic substitution in the *ortho* position of a phenol group [36]. Structural analysis of the radioiodinated derivative has shown that in this way one ^{123}I radionuclide is reproducibly introduced on carbon atom 2, in the *ortho* position of the phenolic group with the most acidic characteristics (Fig. 1). The so-formed mono-[^{123}I]iodohypericin (MIH) could be efficiently separated from the starting material hypericin by reversed phase HPLC and was obtained with more than 99% purity in non-carrier-added form in a yield of 70–97% relative to starting ^{123}I activity.

For a preliminary evaluation of the necrosis-avid characteristics of MIH, only a limited number of animals were included in the present study owing to an increasing appeal for animal protection. However, the meticulous and accurate methodologies applied allow us to conclude that MIH is a highly sensitive necrosis-avid agent which may have future clinical applications. After intravenous injec-

tion in rats, gamma camera images showed MIH to be rapidly distributed over the whole body, with early visualisation of blood pool, liver and kidneys, followed by intestines and to a lesser degree urinary bladder. At 24 h and 48 h after injection, there was clear accumulation of MIH in a well-defined area of the induced liver infarction; by contrast, in the untreated rat, an even distribution throughout the liver region was seen at these time points (Fig. 2). As hypericin and MIH are very lipophilic compounds, it is normal that their excretion via liver and intestines is quite high [36, 40]. For this reason, the clear visualisation of a hot spot in the liver is even more remarkable, indicating a high target to non-target activity ratio. Confirmation that this preferential activity uptake was in the infarcted tissue was obtained by comparison of the images generated with TTC staining, H&E staining and autoradiography of tissue blocks from excised liver lobes after sacrifice of the animal 48 h post injection. There was a perfect match between the distribution of radioactivity seen on the autoradiographic image of infarcted liver tissue and the areas stained with H&E, the latter confirming the presence of necrotic tissue (Fig. 4). The same holds true for the images obtained after staining with TTC (Fig. 3). Comparison of the activity per gram tissue in infarcted liver tissue over that in normal liver tissue reveals a 10-fold higher radioactivity concentration in the infarcted area. This is a clear indication that the new tracer agent MIH indeed has a high affinity for necrotic tissue.

The suitability of MIH for visualisation of necrotic myocardium was confirmed using a rabbit model of myocardial infarction. Also in the rabbit study a remarkable hot spot was visible in the region of the myocardial infarction, both at 24 h and at 48 h post injection (Figs. 5, 6). As in the rat study, a perfect match was found between the areas stained by TTC and the areas with higher uptake of radioactivity. As the heart normally has a low uptake of hypericin and MIH [36, 40], it was a logical finding that the target (necrotic myocardium) to non-target (normal myocardium) radiotracer concentration ratio in selected tissue areas was even higher than in the case of the rat liver, namely by a factor of 18. This ratio could have been even higher had more accurate tissue sampling been performed at the subendocardial region, which is the location of higher activity in this model of occlusive myocardial infarction (Fig. 6).

The in vivo SPECT images obtained from the small animals considered in this study, i.e. rat and rabbit, suffer from limited spatial resolution. The use of micro-SPECT would eliminate this shortcoming, but this technique was not available in our department at the time of this study. However, ex vivo autoradiography in combination with histochemical staining techniques convincingly confirmed the accumulation of MIH in infarcted liver and myocardium. These results suggest that in patients, MIH in combination with SPECT will probably be able to display detailed uptake patterns such as the “doughnut sign”. This implies that MIH-SPECT will be of value in differential diagnosis between occlusive and reperfused myocardial infarction, which is crucial for making clinical decisions regarding prompt interventions for coronary revascularisation [38, 39].

Regarding the mechanisms behind the observed necrosis avidity of MIH and other compounds mentioned in this paper, there exist more hypotheses than solid experimental proofs [1–33, 37–39]. Despite a great diversity in chemical structures and physicochemical properties among the various necrosis-avid tracer agents for nuclear medicine and necrosis-avid contrast agents for MRI, common physicochemical interactions should be shared by at least some of these agents. A careful analysis of the relationship between structure and uptake/retention of the known necrosis-avid agents in necrotic tissue may provide deeper insights into the unique mechanisms of the phenomenon and yield useful information regarding the structural requirements for further optimisation of this type of agent. Moreover, studies are in progress to identify the exact site of binding of MIH in necrotic tissue and to elucidate the influence of structural modifications on its necrosis avidity.

The present preliminary study has surprisingly shown that MIH has pronounced necrosis-avid properties and merits further evaluation as a potentially useful tracer agent for tissue viability assessment and possibly also as a targeting carrier for tissue revival therapies. It is clear, however, that more investigations are needed, especially with respect to the dynamics of uptake, the earliest time point when necrosis becomes visible and the mechanism of uptake in comparison with that of previously reported necrosis-avid tracer agents such as ^{99m}Tc-pyrophosphate and ^{99m}Tc-glucarate. In addition, further optimisation appears to be indicated, e.g. with respect to rate of excretion, solubility of the tracer agent and nature of the radionuclide. In view of the optimal characteristics of ^{99m}Tc, labelling with ^{99m}Tc would be more appropriate and will be included in further studies.

Acknowledgements. The authors wish to thank Peter Vermaelen for his much-appreciated help with the animal imaging studies. The Fund for Scientific Research – Flanders is acknowledged for financial support (research grant G.0257.05).

References

1. Flotats A, Carrió I. Non-invasive in vivo imaging of myocardial apoptosis and necrosis. Eur J Nucl Med Mol Imaging 2003; 30:615–630
2. Buja LM, Tofe AJ, Kulkarni PV, Mukherjee A, Parkey RW, Francis MD, et al. Sites and mechanisms of localization of technetium-99m phosphorous radiopharmaceuticals in acute myocardial infarcts and other tissues. J Clin Invest 1977; 60:724–740
3. Khaw BA, Gold HK, Yasuda T, Leinbach RC, Kanke M, Fallon JT, et al. Scintigraphic quantification of myocardial necrosis in patients after intravenous injection of cardiac myosin specific antibody. Circulation 1986;74:501–508
4. Khaw BA, Yasuda T, Gold HK, Leinbach RC, Johns JA, Kanke M, et al. Acute myocardial infarction imaging with indium-111 labeled monoclonal antimyosin Fab fragments. J Nucl Med 1987;28:1671–1678

5. Khaw BA, Fallon JT, Beller GA, Haber E. Specificity of localization of myosin-specific antibody fragments in experimental myocardial infarction: histologic, histochemical, autoradiographic and scintigraphic studies. Circulation 1979;60: 1527–1531
6. Khaw BA, Scott J, Fallon JT, Cahill SL, Haber E, Homcy C. Myocardial injury: quantitation by cell sorting initiated with antimyosin fluorescent spheres. Science 1982;217:1050–1053
7. Khaw BA. The current role of infarct avid imaging. Semin Nucl Med 1999;29:259–270
8. Frist W, Yasuda T, Segall G, Khaw BA, Strauss HW, Gold H, et al. Noninvasive detection of human cardiac transplant rejection with indium-111 anti-myosin (Fab) imaging. Circulation 1987;76:81–85
9. Ballester M, Obrador D, Carrio I, Auge JM, Moya C, Ponsllado G, et al. ^{111}In-monoclonal antimyosin antibody studies after the first year of heart transplantation: identification of risk groups for developing rejection during long-term follow-up and clinical implications. Circulation 1990;82:2100–2108
10. Olmos RAV, Carrio I, Hoefnagel CA, Estorch M, Huinink WWT, Lopez-Pousa J, et al. High sensitivity of radiolabelled antimyosin scintigraphy in assessing anthracycline related early myocyte damage preceding cardiac dysfunction. Nucl Med Commun 2002;23:871–877
11. Dec GW, Palacios IF, Yasuda T, Fallon JT, Khaw BA, Strauss HW, et al. Antimyosin antibody cardiac imaging: its role in the diagnosis of myocarditis. J Am Coll Cardiol 1990;6:97–104
12. Narula J, Khaw BA, Dec GW, Palacios IF, Southern JF, Fallon JT, et al. Recognition of acute myocarditis masquerading as acute myocardial infarction. N Engl J Med 1992;328:100–104
13. Obrador D, Ballester M, Carrio I, Auge JM, Lopez CM, Bosch I, et al. Active myocardial damage without attending inflammatory response in idiopathic dilated cardiomyopathy. J Am Coll Cardiol 1993;21:1667–1671
14. Obrador D, Ballester M, Carrió I, Moya C, Bosch I, Marti V, et al. Presence, evolving changes, and prognostic implications of myocardial damage detected in idiopathic and alcoholic dilated cardiomyopathy by ^{111}In monoclonal antimyosin antibodies. Circulation 1994;89:2054–2061
15. Narula J, Petrov A, Pak KY, Lister BC, Khaw BA. Very early noninvasive detection of acute experimental nonreperfused myocardial infarction with ^{99m}Tc-labeled glucarate. Circulation 1995;95:1577–1584
16. Khaw BA, Nakazama A, O'Donell SM, Pak KY, Narula J. Avidity of technetium-99m glucarate for the necrotic myocardium: in vivo and in vitro assessment. J Nucl Cardiol 1997; 4:283–290
17. Nelson J, Schmiedl U, Shankland E. Metalloporphyrins as tumor-seeking MRI contrast media and as potential selective treatment sensitizers. Invest Radiol 1990;25:S71–S73
18. Ni Y, Marchal G, Yu J, Lukito G, Petre C, Wevers M, et al. Localization of metalloporphyrin induced "specific" enhancement in experimental liver tumors: a comparison between MRI, microangiographic and histologic findings. Acad Radiol 1995; 2:687–699
19. Ni Y, Petré C, Miao Y, Yu J, Cresens E, Adriaens P, et al. Magnetic resonance imaging–histomorphologic correlation studies on paramagnetic metalloporphyrins in rat models of necrosis. Invest Radiol 1997;32:770–779
20. Maurer J, Strauss A, Ebert W, Bauer H, Felix R. Contrast-enhanced high resolution magnetic resonance imaging of pigmented malignant melanoma using Mn-TPPS4 and Gd-DTPA: experimental results. Melanoma Res 2000;10:40–46
21. Marchal G, Ni Y. Use of porphyrin-complex or expanded porphyrin-complex as an infarction localization diagnosticum. U.S. patent No. 6,013,241. 11 January 2000
22. Marchal G, Ni Y, Herijgers P, Flameng W, Petre C, Bosmans H, et al. Paramagnetic metalloporphyrins: infarct avid contrast agents for diagnosis of acute myocardial infarction by magnetic resonance imaging. Eur Radiol 1996;6:2–8
23. Ni Y, Marchal G, Herijgers P, Flameng W, Petre C, Ebert W, et al. Paramagnetic metalloporphyrins: from enhancers for malignant tumors to markers of myocardial infarcts. Acad Radiol 1996; 3:S395–S377
24. Herijgers P, Laycock SK, Ni Y, Marchal G, Bogaert J, Bosmans H, et al. Localization and determination of infarct size by Gd-mesoporphyrin enhanced MRI in dogs. Int J Cardiac Imaging 1997;13:499–507
25. Ni Y, Pislaru C, Bosmans H, Pislaru S, Miao Y, Van de Werf F, et al. Validation of intracoronary delivery of metalloporphyrin as an in vivo "histochemical staining" for myocardial infarction with MR imaging. Acad Radiol 1998;5:S37–41
26. Stillman AE, Wilke N, Jerosch-Herold M. Myocardial viability. Radiol Clin North Am 1999;37:361
27. Pislaru SV, Ni Y, Pislaru C, Bosmans H, Miao Y, Bogaert J, et al. Noninvasive measurements of infarct size after thrombo lysis with a necrosis-avid MRI contrast agent. Circulation 1999;99:690–696
28. Saeed M, Bremerich J, Wendland MF, Wyttenbach R, Weinmann HJ, Higgins CB. Reperfused myocardial infarction as seen with use of necrosis-specific versus standard extracellular MR contrast media in rats. Radiology 1999;213:247–57
29. Lim TH, Choi SI. MRI of myocardial infarction. J Magn Reson Imaging 1999;10:686–693
30. Wendland MF, Saeed M, Lund G, Higgins CB. Contrast-enhanced MRI for quantification of myocardial viability. J Magn Reson Imaging 1999;10:694–702
31. Choi SI, Choi SH, Kim ST, Lim KH, Lim CH, Gong GY, et al. Irreversibly damaged myocardium at MR imaging with a necrotic tissue-specific contrast agent in a cat model. Radiology 2000;215:863–868
32. Lee SS, Goo HW, Park SB, Lim CH, Gong GY, Seo LB, et al. MR imaging of reperfused myocardial infarction: comparison of necrosis-specific and intravascular contrast agents in a cat model. Radiology 2003;226:739–747
33. Ni Y, Miao Y, Bosmans H, Marchal GJ, Semmler W, Baert AL. Evaluation of interventional liver tumor ablation with Gd-mesoporphyrin enhanced magnetic resonance imaging. Radiology 1997;205:P319
34. Pass HI. Photodynamic therapy in oncology: mechanisms and clinical use. J Natl Cancer Inst 1993;85:443–456
35. Chen B, Zupko I, De Witte PA. Photodynamic therapy with hypericin in a mouse P388 tumor model: vascular effects determine the efficacy. Int J Oncol 2001;18:737–742
36. Vanbilloen H, Bormans G, Chen B, de Witte P, Verbruggen A, Verbeke K. Synthesis and preliminary evaluation of mono-[^{123}I]iodohypericin. J Labelled Compd Radiopharm 2001;44: S965–967
37. Ni Y, Adzamli K, Miao Y, Cresens E, Yu J, Periasamy MP, et al. MRI contrast enhancement of necrosis by MP-2269 and Gadophrin-2 in a rat model of liver infarction. Invest Radiol 2001;36:97–103
38. Ni Y, Dymarkowski S, Chen F, Bogaert J, Marchal G. Occlusive myocardial infarction: enhanced or not enhanced with necrosis avid contrast agents at magnetic resonance imaging. Radiology 2002;225:603–605
39. Rude R, Parkey RW, Bonte FJ, Twieg D, Lewis S, Pulido J, et al. Clinical implications of the "doughnut" pattern of uptake in myocardial imaging with technetium-99m stannous pyrophosphate. Circulation 1977;56:146
40. Lavie G, Mazur Y, Lavie D, Meruelo D. The chemical and biological properties of hypericin: a compound with a broad spectrum of biological activities. Med Res Rev 1995;15:111–119